

# Observation of itinerant gapless excitations in quantum spin liquid $\text{Na}_2\text{BaCo}(\text{PO}_4)_2$

N. Li<sup>1</sup>, W. J. Chu<sup>1</sup>, Q. Huang<sup>2</sup>, Q. Chen<sup>2</sup>, X. Y. Yue<sup>3</sup>, X. Zhao<sup>4</sup>, H. D. Zhou<sup>2\*</sup>, and X. F. Sun<sup>1,3\*</sup>

<sup>1</sup>Department of Physics, Hefei National Laboratory for Physical Sciences at Microscale, and Key Laboratory of Strongly-Coupled Quantum Matter Physics (CAS), University of Science and Technology of China, Hefei, Anhui 230026, People's Republic of China

<sup>2</sup>Department of Physics and Astronomy, University of Tennessee, Knoxville, Tennessee 37996-1200, USA

<sup>3</sup>Institute of Physical Science and Information Technology, Anhui University, Hefei, Anhui 230601, People's Republic of China

<sup>4</sup>School of Physical Sciences, University of Science and Technology of China, Hefei, Anhui 230026, People's Republic of China

\*email: hzhou10@utk.edu; xfsun@ustc.edu.cn

**The most fascinating feature of certain two dimensional (2D) gapless quantum spin liquids (QSL) is that their spinon excitations behave like the fermionic carriers of a paramagnetic metal. The spinon Fermi surface is then expected to produce a linear increase of the thermal conductivity with temperature that should manifest via a residual value ( $\kappa_0/T$ ) in the zero-temperature limit. However, this linear in  $T$  behavior has only been reported for very few QSL candidates that do not include any magnetic oxide. Here we report a residual value of  $\kappa_0/T$  in the effective spin-1/2 triangular antiferromagnet  $\text{Na}_2\text{BaCo}(\text{PO}_4)_2$ . This observation indicates that  $\text{Na}_2\text{BaCo}(\text{PO}_4)_2$  is a gapless QSL.**

The entangled spin state in the celebrated 2D gapless QSL [1-4] can host non-abelian quasiparticle [5] and fractional excitations [6, 7] known as spinons [8, 9], which allows quantum mechanical encryption and transportation of information and makes a potential qubit that is protected against environmental influences [10]. This makes QSL a material platform to potentially solve problems of drastically increased complexities and deliver information with unhackable security needed for quantum computing and quantum information transportation. Through decades of extensive studies on 2D gapless QSL, three experimental hallmarks have been widely accepted as evidence for spinon, including (i) a broad continuous magnetic excitation in the inelastic neutron scattering (INS) spectrum [6, 11, 12]; (ii) a large magnetic specific heat with power law ( $C \sim T^\alpha$ ) temperature dependence [13-15]; and (iii) a non-zero  $\kappa_0/T$  term of ultralow-temperature thermal conductivity [16-19]. While most of the suggested 2D gapless QSLs exhibit the first two hallmarks, they DO NOT exhibit the third one. In reality, so far only the organic  $\text{EtMe}_3\text{Sb}[\text{Pd}(\text{dmit})_2]_2$  with high-quality crystalline form [18, 19] unambiguously shows the non-zero  $\kappa_0/T$  term. For others, actually most of them are magnetic oxides, such as  $\text{YbMgGaO}_4$  with triangular lattice [20] and  $\text{Ca}_{10}\text{Cr}_7\text{O}_{28}$  with bilayer kagome lattice [21], the  $\kappa_0/T$  term tends to be zero upon approaching zero temperature.

Recent theoretical developments on QSLs have proposed that disorder can induce spin-singlet dimers of varying strengths, referred as random singlet (RS) or valence bond glass (VBG) [22-25]. This RS (VBG) state can account not only for the spin-liquid like behaviors, such as a continuum of excitations in the dynamical spin structure factor and the power law specific heat due to its widely distributed binding energy, but also the NON-liquid like behavior, the disappearance of the  $\kappa_0/T$  term due to its glassy nature. Indeed, disorder is unavoidable in most of the studied 2D gapless QSL candidates. For instance,  $\text{YbMgGaO}_4$  has  $\text{Mg}^{2+}/\text{Ga}^{4+}$  site mixture [26];  $\text{Ca}_{10}\text{Cr}_7\text{O}_{28}$  has disorder among the two different  $\text{Cr}^{3+}$  positions [27, 28]; the kagome lattice herbertsmithite  $\text{ZnCu}_3(\text{OH})_6\text{Cl}_2$  has  $\text{Zn}^{2+}/\text{Cu}^{2+}$  site mixture [29] (whether there is a small gap in this QSL candidate is still under debate); the  $\text{LiZn}_2\text{Mo}_3\text{O}_8$  with breathing kagome lattice has  $\text{Li}^+/\text{Zn}^{2+}$  site mixture [30]; and the  $\text{H}_3\text{LiIr}_2\text{O}_6$  with honeycomb lattice has mobile Hydrogen ions [31]. Thermal conductivity data is not available yet for the later three examples. The recently studied triangular lattice  $\text{NaYbO}_2$  with has been claimed to have no site disorder, but this system only exists in polycrystalline form [32]. While the RS picture casts doubts on most of the studied 2D gapless QSLs, the thermal

conductivity seems to be the smoking gun that can be used to discriminate the disorder induced spin-liquid like state from the truly gapless QSL with a spinon Fermi surface.

Recently, Cava's group reported a new Co-based triangular lattice magnet  $\text{Na}_2\text{BaCo}(\text{PO}_4)_2$  [33]. This system has a trigonal crystal structure with lattice parameter  $a = 5.3185 \text{ \AA}$  and  $c = 7.0081 \text{ \AA}$ . The magnetic  $\text{CoO}_6$  octahedra forms a triangular layer in the  $ab$  plane, separated by a layer of nonmagnetic  $\text{BaO}_{12}$  polyhedra. Meanwhile, the  $\text{Na}^+$  ions fill the gaps in the  $\text{CoO}_6$  layers (Figure 1(a, b)). Overall, no site mixture among the ions has been observed. Due to its Kramers ion nature, the  $\text{Co}^{2+}$  ions can be treated as effective spin-1/2 at low temperatures. The magnetic susceptibility, INS spectrum, and specific heat data shows no magnetic ordering down to 0.05 K but with large magnetic specific heat and localized low energy spin fluctuations. Then, as discussed above, to confirm whether it is a truly gapless QSL or a RS state, it is crucial to look for the possible existence of itinerant spinons.

By following Cava's recipe, we grew single crystals of  $\text{Na}_2\text{BaCo}(\text{PO}_4)_2$ . Figure 1(c) shows its inverse of the DC magnetic susceptibility ( $1/\chi$ ) with applied field  $H // ab$  plane. A change of slope is observed around 50 K. The effective moment is estimated to be  $5.37 \mu_B$  for  $150 < T < 300 \text{ K}$  and  $4.0 \mu_B$  for  $2 < T < 20 \text{ K}$  by using the linear Curie-Weiss fittings. This decrease of effective moment indicates a crossover of spin state for  $\text{Co}^{2+}$  ions from high ( $S = 3/2$ ) to low ( $S = 1/2$ ) spin state. Similar behavior has also been observed in other triangular lattice magnets with octahedral Co sites [34, 35]. Therefore, the  $\theta_{\text{CW}} = -2.5 \text{ K}$  obtained at low temperatures fitting represents its intrinsic antiferromagnetic exchange interaction energy level. According to the mean field theory,  $\theta_{\text{CW}}$  is given as  $(-zJS(S+1))/3k_B$ , where  $J$  is the exchange interaction of the Heisenberg Hamiltonian  $J \sum_{(i,j)} S_i S_j$ , and  $z$  is the number of nearest neighbors. For the  $S = 1/2$  triangular lattice with  $z = 6$ , we obtained  $J/k_B = -2/3\theta_{\text{CW}} = 1.7 \text{ K}$ .

Figure 2(a, b) shows the ultralow-temperature thermal conductivity at 0 and 14 T, respectively. Several features are noteworthy. First, both the data are well fitted by  $\kappa/T = \kappa_0/T + bT^2$  with  $b$  as a constant in a very broad temperature range (from several tens to  $\sim 500 \text{ mK}$ ), while the fitting parameters  $\kappa_0/T$  and  $b$  are clearly different for the two sets of data. Second, in zero field the fitting gives  $\kappa_0/T = 0.0062 \text{ W/K}^2\text{m}$ , that is, the presence of a residual value in  $\kappa/T$  while approaching zero temperature is clearly resolved. This residual thermal conductivity immediately implies the excitation is gapless and has a long-range algebraic (power law) temperature dependence. By following Ref.18's method, we estimate the mean free path ( $l_s$ ) and life time of the spin excitation

( $\tau_s$ ) of the quasiparticles responsible for the excitations by calculating  $\frac{\kappa_0}{T} = \frac{\pi k_B^2}{9h} \frac{l_s}{ad} = \frac{\pi}{9} \left(\frac{k_B}{h}\right)^2 \frac{J}{d} \tau_s$ . Here  $a$  ( $\sim 5.32$  Å) and  $d$  ( $\sim 7.01$  Å) are nearest-neighbor and interlayer spin distance, respectively. From the observed  $\kappa_0/T = 0.0062$  W/K<sup>2</sup>m, the  $l_s$  is obtained as 36.6 Å, indicating the excitations are mobile to a distance 7 times as long as the inter-spin distance without being scattered. By using  $J = 1.7$  K, the obtained  $\tau_s$  is  $3.09 \times 10^{-11}$  s. Third, in high magnetic field of 14 T, although the  $\kappa$  is much larger than the zero-field data, the fitting gives a negligibly small value of, or vanishing  $\kappa_0/T$ . It is very reasonable since 14 T is strong enough to polarize all spins and completely suppress the spinon excitations of the QSL state. Thus, the 14 T data should be a result of pure phonon heat transport. From the specific heat data (see the Supplementary materials), it is found that the phonon specific heat can be approximated as  $C_{ph} = \beta T^3$  at very low temperatures with the coefficient  $\beta = 8.83 \times 10^{-4}$  J/K<sup>4</sup>mol. The phonon velocity can be calculated from the  $\beta$  value as  $v_{ph} = 2430$  m/s. The phonon thermal conductivity in the ballistic scattering limit is  $\kappa_{ph} = (1/3)C_{ph}v_{ph}l_{ph}$ , where the phonon mean free path is determined by the averaged sample width of  $l_{ph} = 2\sqrt{A/\pi} = 0.32$  mm for this sample. Thus, the phonon thermal conductivity at low temperature is expected as  $\kappa_{ph} = 2.21 \times T^3$  W/Km. Note that this estimation is different from the 14 T data by only a factor of 2, which is acceptable. If one assume the 14 T data is purely phonon term, much smaller data in zero field indicates that the phonon ballistic scattering limit is not achieved although they show a pretty good behavior of  $\kappa_0/T + bT^2$ . Therefore, the phonons are always suffering some scattering effect besides the boundary in zero field. Apparently, at very low temperatures only the magnetic excitations can be acted as this role of phonon scattering.

Figure 3(a) shows the zero-field thermal conductivity of Na<sub>2</sub>BaCo(PO<sub>4</sub>)<sub>2</sub> in temperature range of 70 mK – 30 K. It behaves like a usual insulating crystal. The peak at 12 K with rather large value of 90 W/Km can be understood as the so-called phonon peak. As shown are the thermal conductivity in 14 T magnetic field, which can increase the  $\kappa$  at temperatures up to 7 K. Figure 3(b) shows the magnetic field dependence of  $\kappa$  at 380 and 850 mK. Both of them show a rather simple behavior, that is, the  $\kappa$  increases quickly at low field and saturates at field above 3 T. It has a good correspondence to the spin polarization behavior revealed by the magnetization curves [33]. These results, again, clearly indicate that in zero field the phonons are rather strongly scattered by the spinon excitations of the QSL state and the high field can suppress the spinons and the scattering effect as well.

In summary, we clearly observed a nonzero residual thermal conductivity  $\kappa_0/T$  in the *inorganic* QSL candidates for the first time. It is well known that the residual thermal conductivity in the zero-temperature limit demonstrates that the excitation from the ground state is gapless, and the associated correlation function has a long-range algebraic (power-law) dependence. This experimental result provides a clear evidence that  $\text{Na}_2\text{BaCo}(\text{PO}_4)_2$  has a QSL ground state with gapless spinon excitations. Till now the nonzero  $\kappa_0/T$  has been only observed in high-quality *organic* QSL candidate,  $\text{EtMe}_3\text{Sb}[\text{Pd}(\text{dmit})_2]_2$ . In comparison, the  $\kappa_0/T$  value of  $\text{Na}_2\text{BaCo}(\text{PO}_4)_2$  is much ( $\sim 30$  times) smaller than that of  $\text{EtMe}_3\text{Sb}[\text{Pd}(\text{dmit})_2]_2$ , which may be attributed to two possible reasons. First, the spinon velocity is much smaller in  $\text{Na}_2\text{BaCo}(\text{PO}_4)_2$  due to the small  $J$  value. Second, the  $\tau_s$  is similar to that of the organic sample but the  $l_s$  is much shorter in  $\text{Na}_2\text{BaCo}(\text{PO}_4)_2$ , which is related to stronger scattering between phonon and spinon.

## References

- [1] Balents, L. Spin liquids in frustrated magnets. *Nature* **464**, 199-208 (2010).
- [2] Savary, L., & Balents, L. Quantum spin liquids: a review. *Rep. Prog. Phys.* **80**, 016502 (2016).
- [3] Zhou, Y., Kanoda, K., & Ng, T. K. Quantum spin liquid states. *Rev. Mod. Phys.* **89**, 025003 (2017).
- [4] Knolle, J., & Moessner, R. A field guide to spin liquids. *Annual Review of Condensed Matter Physics* **10**, 451-472 (2019).
- [5] Nayak, C., Simon, S. H., Stern, A., Freedman, M., & Sarma, S. D. Non-Abelian anyons and topological quantum computation. *Rev. Mod. Phys.* **80**, 1083-1159 (2008).
- [6] Han, T. H., Helton, J. S., Chu, S., Nocera, D. G., Rodriguez-Rivera, J. A., Broholm, C., & Lee, Y. S. Fractionalized excitations in the spin-liquid state of a kagome-lattice antiferromagnet. *Nature* **492**, 406-410 (2012).
- [7] Punk, M., Chowdhury, D., & Sachdev, S. Topological excitations and the dynamic structure factor of spin liquids on the kagome lattice. *Nat. Phys.* **10**, 289-293 (2014).
- [8] Kohno, M., Starykh, O. A., & Balents, L. Spinons and triplons in spatially anisotropic frustrated antiferromagnets. *Nat. Phys.* **3**, 790-795 (2007).
- [9] Nussinov, Z., Batista, C. D., Normand, B., & Trugman, S. A. High-dimensional fractionalization and spinon deconfinement in pyrochlore antiferromagnets. *Phys. Rev. B* **75**, 094411 (2007).

- [10] Kitaev, A., & Preskill, J. Topological Entanglement Entropy. *Phys. Rev. Lett.* **96**, 110404 (2006).
- [11] Shen, Y. *et al.*, Evidence for a spinon Fermi surface in a triangular lattice quantum-spin-liquid candidate. *Nature* **540**, 559-562 (2016).
- [12] Paddison, J. A. *et al.*, Continuous excitations of the triangular-lattice quantum spin-liquid YbMgGaO<sub>4</sub>. *Nat. Phys.* **13**, 117-122 (2017).
- [13] Yamashita, S. *et al.* Thermodynamic properties of a spin-1/2 spin-liquid state in a  $\kappa$ -type organic salt. *Nat. Phys.* **4**, 459-462(2008).
- [14] Motrunich, O. I. Variational study of triangular lattice spin-1/2 model with ring exchanges and spin liquid state in  $\kappa$ -(ET)<sub>2</sub>Cu<sub>2</sub>(CN)<sub>3</sub>. *Phys. Rev. B* **72**, 045105 (2005).
- [15] Lee, S. S., & Lee, P. A. U(1) gauge theory of the Hubbard model: Spin liquid states and possible application to  $\kappa$ -(BEDT-TTF)<sub>2</sub>Cu<sub>2</sub>(CN)<sub>3</sub>. *Phys. Rev. Lett.* **95**, 036403 (2005).
- [16] Nave, C. P., & Lee, P. A. Transport properties of a spinon Fermi surface coupled to a U(1) gauge field. *Phys. Rev. B* **76**, 235124 (2007).
- [17] Werman, Y., Chatterjee, S., Morampudi, S. C., & Berg, E. Signatures of Fractionalization in Spin Liquids from Interlayer Thermal Transport. *Phys. Rev. X* **8**, 031064 (2018).
- [18] Yamashita, M. *et al.* Highly mobile gapless excitations in a two-dimensional candidate quantum spin liquid. *Science* **328**, 1246-1248 (2010).
- [19] Yamashita, M. Boundary-limited and Glassy-like Phonon Thermal Conduction in EtMe<sub>3</sub>Sb[Pd(dmit)<sub>2</sub>]<sub>2</sub>. *J. Phys. Soc. Jpn.* **88**, 083702 (2019).
- [20] Xu, Y. *et al.* Absence of magnetic thermal conductivity in the quantum spin-liquid candidate YbMgGaO<sub>4</sub>. *Phys. Rev. Lett.* **117**, 267202 (2016).
- [21] Ni, J. M. *et al.* Ultralow-temperature heat transport in the quantum spin liquid candidate Ca<sub>10</sub>Cr<sub>7</sub>O<sub>28</sub> with a bilayer kagome lattice. *Phys. Rev. B* **97**, 104413 (2018).
- [22] Bhatt, R. N., & Lee, P. A. Scaling studies of highly disordered spin-1/2 antiferromagnetic systems. *Phys. Rev. Lett.* **48**, 344-347 (1982).
- [23] Paalanen, M. A. *et al.* Thermodynamic behavior near a metal-insulator transition. *Phys. Rev. Lett.* **61**, 597-600 (1988).
- [24] Kimchi, I., Nahum, A., & Senthil, T. Valence bonds in random quantum magnets: theory and application to YbMgGaO<sub>4</sub>. *Phys. Rev. X* **8**, 031028 (2018).

- [25] Kimchi, I. *et al.* Scaling and data collapse from local moments in frustrated disordered quantum spin systems. *Nat. Commun.* **9**, 4367 (2018).
- [26] Li, Y. *et al.* Gapless quantum spin liquid ground state in the two-dimensional spin-1/2 triangular antiferromagnet  $\text{YbMgGaO}_4$ . *Sci. Rep.* **5**, 16419 (2015).
- [27] Balz, C. *et al.* Physical realization of a quantum spin liquid based on a complex frustration mechanism. *Nat. Phys.* **12**, 942-949 (2016).
- [28] Balz, C. *et al.* Crystal growth, structure and magnetic properties of  $\text{Ca}_{10}\text{Cr}_7\text{O}_{28}$ . *J. Phys.: Condens. Matt.* **29**, 225802 (2017).
- [29] Han, T. H. *et al.* Correlated impurities and intrinsic spin-liquid physics in the kagome material herbertsmithite. *Phys. Rev. B* **94**, 060409 (2016).
- [30] Sheckelton, J. P., Neilson, J. R., Soltan, D. G., & McQueen, T. M. Possible valence-bond condensation in the frustrated cluster magnet  $\text{LiZn}_2\text{Mo}_3\text{O}_8$ . *Nat. Mater.* **11**, 493-496 (2012).
- [31] Kitagawa, K. *et al.* A spin-orbital-entangled quantum liquid on a honeycomb lattice. *Nature* **554**, 341-345 (2018).
- [32] Bordelon, M. *et al.* Field-tunable quantum disordered ground state in the triangular-lattice antiferromagnet  $\text{NaYbO}_2$ . *Nat. Phys.* **15**, 1058-1064 (2019).
- [33] Zhong, R. D. *et al.* Strong quantum fluctuations in a quantum spin liquid candidate with a Co-based triangular lattice. *Proc. Natl. Acad. Sci.* **116**, 14505-14510 (2019).
- [34] Zhou, H. D. *et al.* Successive Phase Transitions and Extended Spin-Excitation Continuum in the  $S=1/2$  Triangular-Lattice Antiferromagnet  $\text{Ba}_3\text{CoSb}_2\text{O}_9$ . *Phys. Rev. Lett.* **109**, 267206 (2012).
- [35] Lee, M. *et al.* Series of phase transitions and multiferroicity in the quasi-two-dimensional spin-1/2 triangular-lattice antiferromagnet  $\text{Ba}_3\text{CoNb}_2\text{O}_9$ . *Phys. Rev. B* **89**, 104420 (2014).

## Acknowledgements

The work at the University of Science and Technology of China (N.L., W.J.C., X.Z. and X.F.S.) was supported by the National Natural Science Foundation of China (Grants No. U1832209, No. 11874336, and No. 11574286), the National Basic Research Program of China (Grants No. 2015CB921201 and No. 2016YFA0300103), the Innovative Program of Development Foundation of Hefei Center for Physical Science and Technology, and Users with Excellence Project of Hefei Science Center CAS (Grant No. 2018HSC-UE012). The work at the University of Tennessee (Q.H., Q.C. and H.D.Z.) was supported by the National Science Foundation through award DMR-

1350002. Q.H. and H.D.Z. are very grateful to Ruidan Zhong for her helpful discussion on sample synthesis.

### **Author contributions**

N.L. and W.J.C. and X.F.S. performed thermal conductivity measurements and analyzed the data with help from X.Z. and H.D.Z. X.Y.Y. performed the specific heat measurements. Q.H., Q.C. and H.D.Z. made and characterized the samples. X.F.S. and H.D.Z. wrote the paper with input from all other co-authors.



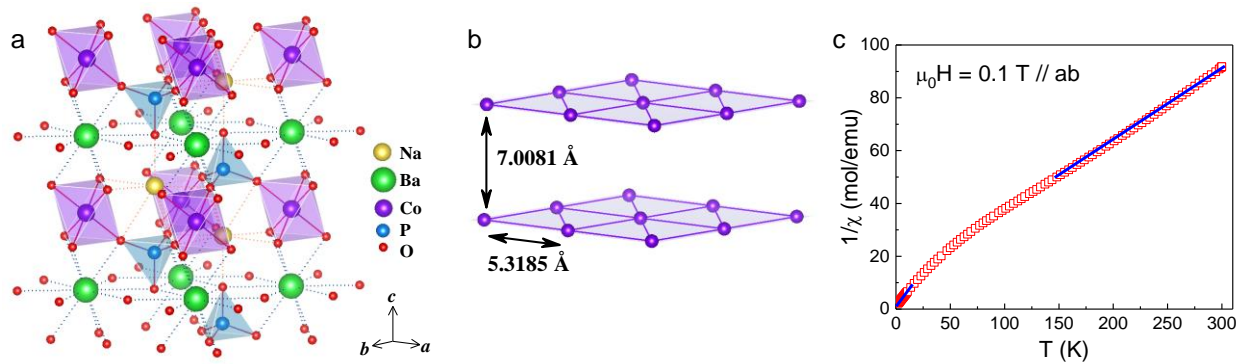


**Figure 1** Structure and magnetic susceptibility of  $\text{Na}_2\text{BaCo}(\text{PO}_4)_2$ . **a**, The crystallographic structure. **b**, The triangular lattice of  $\text{Co}^{2+}$  ions in the  $ab$  plane. **c**, The inverse of the DC susceptibility measured with 0.1 T magnetic field along the  $ab$  plane. The solid lines are the Curie-Weiss fittings to high-temperature or low-temperature data.

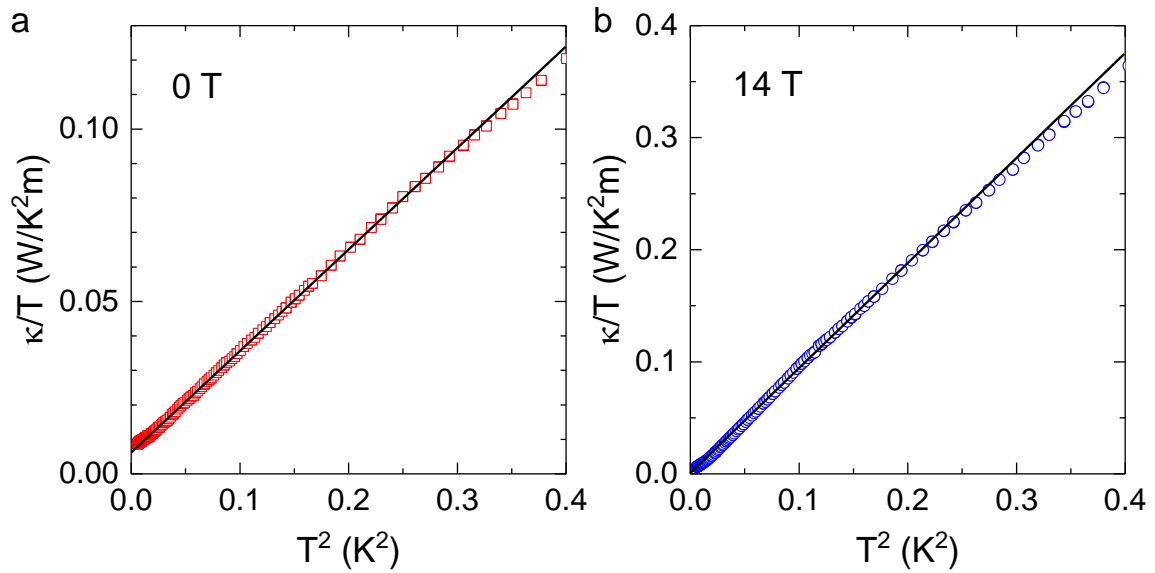


**Figure 2** Ultra-low temperature thermal conductivity of  $\text{Na}_2\text{BaCo}(\text{PO}_4)_2$ . **a**, Data in zero field plotted in  $\kappa/T$  vs  $T^2$ . The solid line is a linear fitting for data at  $T < 550$  mK. A non-zero residual thermal conductivity of  $\kappa_0/T = 0.0062$  W/K<sup>2</sup>m is resolved. **b**, Data in 14 T magnetic field. The solid line is a linear fitting for data at  $T < 450$  mK. There is no residual term ( $\kappa_0/T = 0$ ). The heat current is along the  $a$  axis while the magnetic field is along the  $c$  axis.

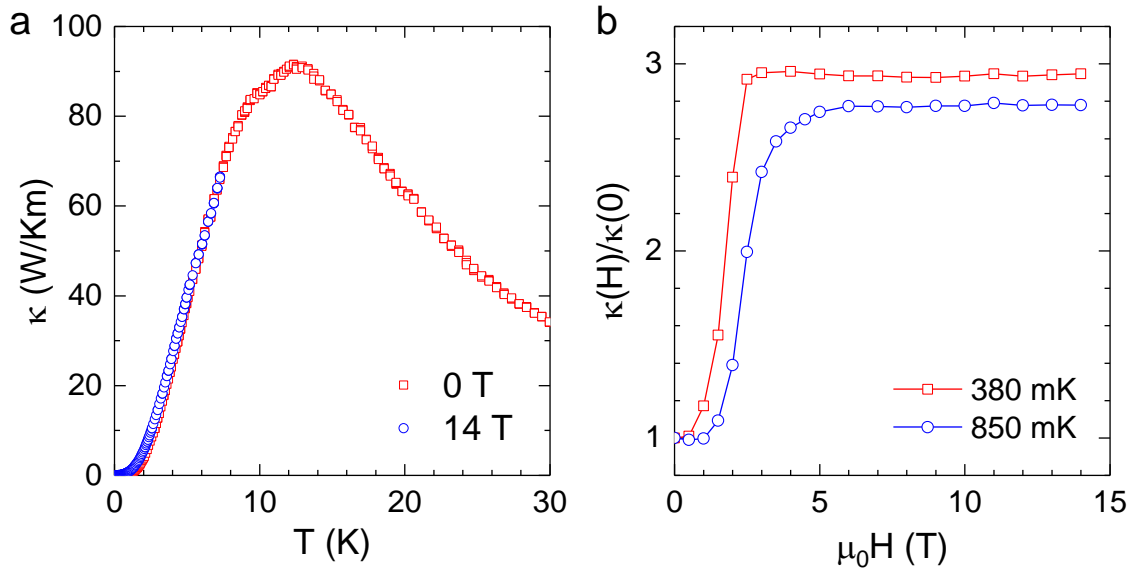


**Figure 3 Thermal conductivity of  $\text{Na}_2\text{BaCo}(\text{PO}_4)_2$ .** **a**, Zero-field thermal conductivity in a wide temperature range from 70 mK to 30 K. Also shown are the thermal conductivity in 14 T magnetic field and at temperatures from 70 mK to 7 K. **b**, Magnetic-field dependence of thermal conductivity at 380 and 850 mK. The heat current is along the  $a$  axis while the magnetic field is along the  $c$  axis.

## Methods

### Sample preparation and characterization

The single crystals were grown by flux method as reported in Reference [33]. One adjustment made is that Platinum crucible instead of alumina crucible was used in our growth. The powder X-ray diffraction measurement on the ground single crystals confirmed its lattice structure is the same as the reported on in Reference [33]. The Laue back diffraction confirmed the flat surface of the as grown crystals is the  $ab$  plane. The DC magnetic susceptibility was measured with a quantum-design superconducting quantum interference device (SQUID) magnetometer. The applied field  $\mu_0 H = 0.1$  T is parallel to the  $ab$  plane. The specific heat was measured with a Quantum Design physical property measurements system (PPMS).

### Thermal conductivity measurements

Thermal conductivity was measured by using a “one heater, two thermometers” technique in a  $^3\text{He}/^4\text{He}$  dilution refrigerator and a  $^3\text{He}$  refrigerator, equipped with a 14 T superconducting magnet [36-40]. The sample was cut precisely along the crystallographic axes with dimensions of  $3.0 \times 0.63 \times 0.14$  mm<sup>3</sup>, where the longest and the shortest dimensions are along the  $a$  and the  $c$  axes, respectively. The heat currents were applied along the  $a$  axis while the magnetic fields were applied along the  $c$  axis.

The residual thermal conductivity  $\kappa_0/T$  in zero field is 0.0062 W/K<sup>2</sup>m, which is  $\sim 30$  times smaller than that observed in organic QSL candidate EtMe<sub>3</sub>Sb[Pd(dmit)<sub>2</sub>]<sub>2</sub> [18]. One may ask whether this value is too small to be resolved by the  $\kappa$  measurement at ultra-low temperatures. We would like to mention that this residual thermal conductivity is actually comparable to those in high-T<sub>c</sub> cuprate superconductors (HTSC). For HTSC, the  $\kappa_0/T$  is contributed by the nodal quasiparticles from the  $d$ -wave superconducting state and has been experimentally observed by us in many materials, including La<sub>2-x</sub>Sr<sub>x</sub>CuO<sub>4</sub>, YBaCu<sub>3</sub>O<sub>y</sub>, Bi<sub>2</sub>Sr<sub>2-x</sub>La<sub>x</sub>CuO<sub>6+ $\delta$</sub> , and Bi<sub>2</sub>Sr<sub>2</sub>CaCu<sub>2</sub>O<sub>8+ $\delta$</sub>  [37-40]. In these materials, it is well resolved that the  $\kappa_0/T$  varies from 0.0015 to 0.06 W/K<sup>2</sup>m and shows systematic changes with the carrier concentration. Similar experimental results have also been reported by other groups for both the cuprate and the iron-based superconductors [41-44]. Therefore, a  $\kappa_0/T$  value of 0.0062 W/K<sup>2</sup>m is big enough to be correctly detected by a high-level measurement.

## References

- [36] Rao, X. *et al.* Quantum oscillation of thermal conductivity and violation of Weidemann-Franz law in TaAs<sub>2</sub> and NbAs<sub>2</sub>. ArXiv:1906.03961.
- [37] Takeya, J., Ando, Y., Komiya, S., & Sun, X. F. Low-Temperature Electronic Heat Transport in La<sub>2-x</sub>Sr<sub>x</sub>CuO<sub>4</sub> Single Crystals: Unusual Low-Energy Physics in the Normal and Superconducting States. *Phys. Rev. Lett.* **88**, 077001 (2002).
- [38] Sun, X. F., Segawa, K., & Ando, Y. Metal-to-Insulator Crossover in YBa<sub>2</sub>Cu<sub>3</sub>O<sub>y</sub> Probed by Low-Temperature Quasiparticle Heat Transport. *Phys. Rev. Lett.* **93**, 107001 (2004).
- [39] Ando, Y. *et al.* Quantum Phase Transitions in the Cuprate Superconductor Bi<sub>2</sub>Sr<sub>2-x</sub>La<sub>x</sub>CuO<sub>6+δ</sub>. *Phys. Rev. Lett.* **92**, 247004 (2004).
- [40] Sun, X. F. *et al.* Electronic Inhomogeneity and Breakdown of the Universal Thermal Conductivity of Cuprate Superconductors. *Phys. Rev. Lett.* **96**, 017008 (2006).
- [41] Hawthorn, D. G. *et al.* Field-Induced Thermal Metal-to-Insulator Transition in Underdoped La<sub>2-x</sub>Sr<sub>x</sub>CuO<sub>4+δ</sub>. *Phys. Rev. Lett.* **90**, 197004 (2003).
- [42] Sutherland, M. *et al.* Thermal conductivity across the phase diagram of cuprates: Low-energy quasiparticles and doping dependence of the superconducting gap. *Phys. Rev. B* **67**, 174520 (2003).
- [43] Doiron-Leyraud, N. *et al.* Onset of a Boson Mode at the Superconducting Critical Point of Underdoped YBa<sub>2</sub>Cu<sub>3</sub>O<sub>y</sub>. *Phys. Rev. Lett.* **97**, 207001 (2006).
- [44] Qiu, X. *et al.* Robust Nodal Superconductivity Induced by Isovalent Doping in Ba(Fe<sub>1-x</sub>Ru<sub>x</sub>)<sub>2</sub>As<sub>2</sub> and BaFe<sub>2</sub>(As<sub>1-x</sub>P<sub>x</sub>)<sub>2</sub>. *Phys. Rev. X* **2**, 011010 (2012).

## Supplementary Information

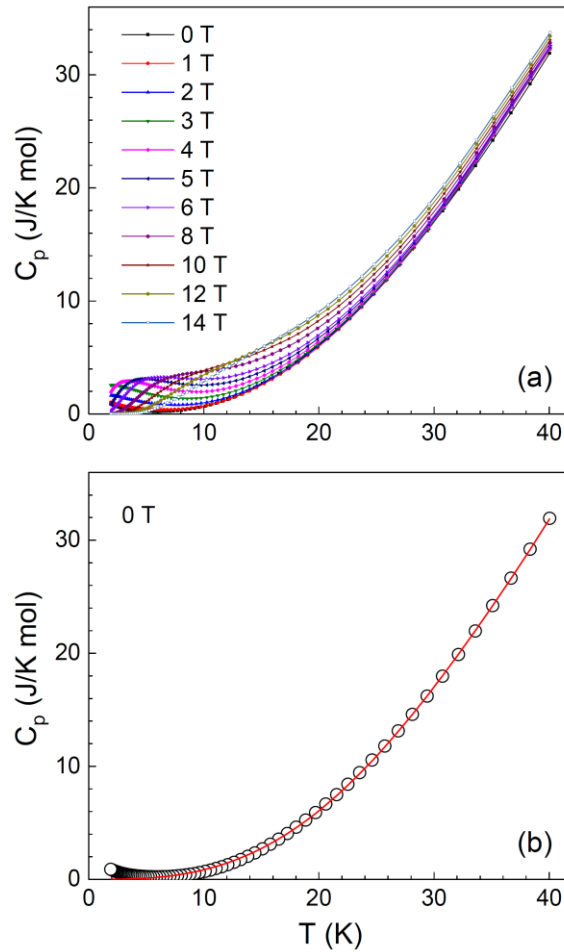


**Figure S1** (a) Specific heat of  $\text{Na}_2\text{BaCo}(\text{PO}_4)_2$  single crystal at 1.9 – 40 K and in various magnetic fields up to 14 T. (b) Zero-field data. The solid line shows the fitting to data at  $T > 10\text{ K}$  by using the formula of phonon specific heat,  $C_{\text{ph}} = \beta T^3 + \beta_5 T^5 + \beta_7 T^7$ .

Figure S1(a) shows the specific heat data of  $\text{Na}_2\text{BaCo}(\text{PO}_4)_2$  single crystal at 1.9 – 40 K and in various magnetic fields of 0 – 14 T. These data are consistent with those reported in by Cava's group [S1]. There is no sign of phase transition in this temperature range. With applying magnetic field, a broad peak appears at low temperature. To estimate the phonon specific heat, we fit the zero-field data at 10 – 40 K by using the low-frequency expansion of the Debye function,  $C_{\text{ph}} = \beta T^3 + \beta_5 T^5 + \beta_7 T^7 + \dots$ , where  $\beta$ ,  $\beta_5$ , and  $\beta_7$  are temperature-independent coefficients [S2], as shown by the solid line in Fig. S1(b). The fitting parameters are  $\beta = 8.83 \times 10^{-4}\text{ J/K}^4\text{mol}$ ,  $\beta_5 = -3.32 \times 10^{-$

$^7 \text{ J/K}^6\text{mol}$ , and  $\beta_7 = 6.67 \times 10^{-11} \text{ J/K}^8\text{mol}$ . Note that at very low temperatures, the  $T^5$  and  $T^7$  terms are negligible and the phonon specific heat shows a well-known  $T^3$  dependence with the coefficient of  $\beta$ .

### Supplementary References

[S1] Zhong, R. D. *et al.* Strong quantum fluctuations in a quantum spin liquid candidate with a Co-based triangular lattice. *Proc. Natl. Acad. Sci.* **116**, 14505-14510 (2019).

[S2] Tari, A. *Specific Heat of Matter at Low Temperatures Ch. 2* (Imperial College Press, London, 2003).